Inelastic Raman scattering of light by hydrogenlike ions

T. Jahrsetz,[1,2,*] S. Fritzsche,[2,3] and A. Surzhykov[2]
[1]*Physikalisches Institut, Ruprecht-Karls-Universität Heidelberg, D-69120 Heidelberg, Germany*
[2]*Helmholtz-Institut Jena, D-07743 Jena, Germany*
[3]*Theoretisch-Physikalisches Institut, Friedrich-Schiller-Universität Jena, D-07743 Jena, Germany*
(Received 10 March 2014; published 7 April 2014)

The inelastic Raman scattering of light by hydrogenlike ions has been studied by means of second-order perturbation theory and the relativistic Coulomb Green's-function approach. In particular, we investigate the total and angle-differential Raman cross sections as well as the magnetic sublevel population of the residual (excited) ions. Detailed calculations are performed for the inelastic scattering of photons by neutral hydrogen as well as hydrogenlike xenon and uranium ions, accompanied by the $1s_{1/2} \to 2s_{1/2}$, $1s_{1/2} \to 2p_{1/2}$, and $1s_{1/2} \to 2p_{3/2}$ transitions. Moreover, we discuss how the Raman scattering is affected by relativistic and resonance effects as well as the higher-multipole contributions to the electron-photon interaction.

DOI: 10.1103/PhysRevA.89.042501 PACS number(s): 31.10.+z, 32.80.Wr, 31.30.jc

I. INTRODUCTION

The inelastic scattering of photons on atoms, ions, or molecules often leads to an excitation of the target. Since the 1920s, this so-called Raman scattering [1,2] has been explored intensively by both experiments and theoretical studies. In atomic physics, most of the investigations have dealt with hydrogen and neutral atoms (see [3]). For these systems, nonrelativistic calculations were performed especially for the total as well as angle-differential Raman cross sections [4–8] and were found to be in good agreement with experimental data [9,10]. The computations also helped to improve our understanding of the spectra of double stars [11,12]. Furthermore, in recent years it was found that the Raman process is a relevant factor in understanding the incoherent and coherent x-ray scattering by neutral atoms [13–15].

In contrast to neutral atoms, less attention has been paid so far to the inelastic photon scattering by highly charged ions. Owing to the recent advances in storage ring and trapping techniques as well as in developing coherent light sources, the scattering of light by ionic targets has become feasible today. When performed with medium- and high-Z targets, these experiments can provide valuable information about the electron-photon interaction and the structure of simple atomic systems in the presence of strong Coulomb fields [16]. Therefore, in order to support the present (as well as future) measurements on the inelastic scattering of light by highly charged ions, theoretical investigations are needed beyond the previously applied nonrelativistic dipole approximation [4–8]. The first steps in this direction were made by Manakov *et al.* [17]. In this work we present a more detailed fully relativistic analysis of the Raman process for hydrogenlike systems. We here restrict our investigation to one-electron ions since they allow us to focus on the major relativistic and nondipole phenomena, leaving the many-electron effects for future case studies.

In the present work we describe inelastic scattering of photons by hydrogenlike ions within the framework of second-order perturbation theory and Dirac's relativistic equation. In this framework, all properties of the Raman process can be readily expressed in terms of two-photon transition amplitudes, as discussed in Sec. II below. These relativistic amplitudes are used to build the total and angle-differential scattering cross sections as well as the alignment parameters of residual (excited) ions and contain also the higher-order multipoles of the radiation field. For all numerical computations of these properties, we use the Coulomb Green's-function method discussed in Sec. III. It is applied to the inelastic Raman scattering of light by neutral hydrogen as well as by hydrogenlike xenon (Xe^{53+}) and uranium (U^{91+}) ions (see Sec. IV). Particular attention is paid to the excitation of the target atoms (and ions) from their ground state to the $2s_{1/2}$, $2p_{1/2}$, and $2p_{3/2}$ levels by photons with energies below the $1s$ ionization threshold. For these photon energies, we here analyze the relativistic and nondipole corrections to the Raman cross sections and the ionic alignment parameters and focus especially on the (resonance) effects arising for the scattering via the resonant excitation and subsequent decay of a real intermediate state. Finally, a brief summary of our findings and an outlook are given in Sec. V.

Hartree atomic units ($\hbar = e = m_e = 1$) are used throughout the paper unless stated otherwise.

II. THEORY

A. Evaluation of the transition amplitude

The scattering of photons by atoms and ions is usually described in terms of second-order perturbation theory [4,5,8]. In this approach, all properties of the scattered light and the residual (atomic) target can be traced back to the two-photon transition amplitude. For Raman scattering involving the excitation of hydrogenlike ions from an initial state $|n_i j_i \mu_i\rangle$ to some final state $|n_f j_f \mu_f\rangle$, this amplitude

*jahrsetz@physi.uni-heidelberg.de

reads

$$M_{if}(\mu_i,\mu_f) = \sum_{n_v j_v \mu_v} \frac{\langle n_f j_f \mu_f | \hat{R}_2^\dagger(\boldsymbol{k}_2,\boldsymbol{\epsilon}_2) | n_v j_v \mu_v \rangle \langle n_v j_v \mu_v | \hat{R}_1(\boldsymbol{k}_1,\boldsymbol{\epsilon}_1) | n_i j_i \mu_i \rangle}{E_i + \omega_1 - E_v} + \sum_{n_v j_v \mu_v} \frac{\langle n_f j_f \mu_f | \hat{R}_1(\boldsymbol{k}_1,\boldsymbol{\epsilon}_1) | n_v j_v \mu_v \rangle \langle n_v j_v \mu_v | \hat{R}_2^\dagger(\boldsymbol{k}_2,\boldsymbol{\epsilon}_2) | n_i j_i \mu_i \rangle}{E_i - \omega_2 - E_v}. \quad (1)$$

Here $\boldsymbol{k}_{1,2}$ and $\boldsymbol{\epsilon}_{1,2}$ are the wave and polarization vectors of the incident and scattered photons, respectively. The energies of these photons $\omega_{1,2} = k_{1,2}/\alpha$ are of course linked to the energies of the initial and final ionic states

$$\omega_2 = \omega_1 - E_f + E_i \quad (2)$$

due to the conservation of energy.

The operator $\hat{R}_1(\boldsymbol{k}_1,\boldsymbol{\epsilon}_1)$ in Eq. (1) describes the absorption of the first (incoming) photon and $\hat{R}_2^\dagger(\boldsymbol{k}_2,\boldsymbol{\epsilon}_2)$ describes the emission of the second (scattered or outgoing) photon. As usual in atomic theory, the transition amplitude $M_{if}(\mu_i,\mu_f)$ can be further evaluated by a decomposition of the operators $\hat{R}_{1,2}^{(\dagger)}$ into their partial wave components, which, within the Coulomb gauge, can be written as

$$\hat{R}_i(\boldsymbol{k}_i,\boldsymbol{\epsilon}_i) = 4\pi \sum_{p_i L_i M_i} i^{L_i - p_i} \left[\boldsymbol{\epsilon}_i \boldsymbol{Y}^{(p_i)*}_{L_i M_i}(\hat{\boldsymbol{k}}_i)\right] \boldsymbol{\alpha} \hat{\boldsymbol{a}}^{p_i}_{L_i M_i}(k_i), \quad (3)$$

where $\boldsymbol{Y}^{(p)}_{LM}(\hat{\boldsymbol{k}})$ denotes a vector spherical harmonic [18], $\hat{\boldsymbol{a}}^p_{LM}$ is the multipole field component of the multipole (p,L,M) [19,20], and $\boldsymbol{\alpha} = (\alpha_x,\alpha_y,\alpha_z)$ refers to the vector of the Dirac matrices. In Eq. (3), moreover, the index L specifies the order of the multipoles, while p distinguishes between the electric ($p = 1$) and magnetic ($p = 0$) transitions. Using this notation, the pair $(p = 1, L = 1)$ refers to the electric dipole $E1$ component of the electron-photon interaction, the pair $(p = 0, L = 1)$ to the magnetic dipole $M1$ component, and so on.

If we insert the expansion (3) into Eq. (1) and perform some simple Racah algebra, the two-photon transition amplitude can be put into the form [19,21–23]

$$M_{if}(\mu_i,\mu_f) = \sum_{kq} \sqrt{2k+1} \langle kq j_f \mu_f | j_i \mu_i \rangle \times U_{kq}(n_f j_f; n_i j_i), \quad (4)$$

where the irreducible tensor $U_{kq}(n_f j_f; n_i j_i)$ of rank k is given by

$$U_{kq}(n_f j_f; n_i j_i) = \sum_{p_1 L_1 p_2 L_2} \frac{(4\pi)^2}{\sqrt{2j_i+1}} (-1)^{j_f + j_i} i^{L_1 + p_1 - L_2 - p_2} T^{L_1 p_1 L_2 p_2}_{kq}(\hat{\boldsymbol{k}}_1, \hat{\boldsymbol{k}}_2) \times \sum_{j_v} \left(\begin{Bmatrix} L_1 & L_2 & k \\ j_f & j_i & j_v \end{Bmatrix} S^{21}_{j_v}(\omega_1) + (-1)^{L_1 + L_2 + k} \begin{Bmatrix} L_1 & L_2 & k \\ j_i & j_f & j_v \end{Bmatrix} S^{12}_{j_v}(-\omega_2) \right). \quad (5)$$

This expression allows for the factorization of the matrix element $M_{if}(\mu_i,\mu_f)$ into (i) a radial part and (ii) a term that depends on the propagation directions $\boldsymbol{k}_{1,2}$ as well as the polarization vectors $\boldsymbol{\epsilon}_{1,2}$ of the photons. The latter term is usually represented by the so-called angular polarization tensor

$$T^{L_1 p_1 L_2 p_2}_{kq}(\hat{\boldsymbol{k}}_1, \hat{\boldsymbol{k}}_2) = \sum_{M_1 M_2} \langle L_1 M_1 L_2 M_2 | kq \rangle \times \left[\boldsymbol{\epsilon}_1 \boldsymbol{Y}^{(p_1)}_{L_1 M_1}(\hat{\boldsymbol{k}}_1)\right] \left[\boldsymbol{\epsilon}_2{}^* \boldsymbol{Y}^{(p_2)}_{L_2 M_2}(\hat{\boldsymbol{k}}_2)\right], \quad (6)$$

whose evaluation in terms of the spherical harmonics was discussed in detail in previous works [19,22,23]. In contrast, the radial integrals enter the amplitude (4) via the reduced matrix elements

$$S^{12}_{j_v}(-\omega_2) \equiv S^{12}_{j_v}(-\omega_2; L_1 p_1, L_2 p_2) = \sum_{n_v} \frac{\langle n_f j_f || \boldsymbol{\alpha} \hat{\boldsymbol{a}}^{p_1}_{L_1} || n_v j_v \rangle \langle n_v j_v || \boldsymbol{\alpha} \hat{\boldsymbol{a}}^{p_2}_{L_2} || n_i j_i \rangle}{E_i - \omega_2 - E_v}, \quad (7)$$

$$S^{21}_{j_v}(\omega_1) \equiv S^{21}_{j_v}(\omega_1; L_1 p_1, L_2 p_2) = \sum_{n_v} \frac{\langle n_f j_f || \boldsymbol{\alpha} \hat{\boldsymbol{a}}^{p_2}_{L_2} || n_v j_v \rangle \langle n_v j_v || \boldsymbol{\alpha} \hat{\boldsymbol{a}}^{p_1}_{L_1} || n_i j_i \rangle}{E_i + \omega_1 - E_v}, \quad (8)$$

which are the standard building blocks for describing different atomic two-photon processes [24]. The computation of these matrix elements is a complicated task since it requires the summation over the complete Dirac spectrum of the ion. In Sec. III we will explain how this summation can be carried out with the aid of the Green's-function approach.

B. Differential and total cross sections

Making use of the second-order amplitude $M_{if}(\mu_i,\mu_f)$ and its radial-angular representation, we can now calculate various properties for the inelastic scattering of photons by hydrogenlike ions. For example, the angle-differential cross section for $|n_i j_i\rangle + \gamma \to |n_f j_f\rangle + \gamma'$ Raman scattering can be obtained from Eqs. (4)–(8) as

$$\frac{d\sigma}{d\Omega}(\theta,\omega_1) = \frac{1}{2}\frac{\omega_2}{\omega_1}\frac{1}{2j_i+1} \sum_{\boldsymbol{\epsilon}_1 \boldsymbol{\epsilon}_2} \sum_{\mu_i,\mu_f} |M_{if}(\mu_i,\mu_f)|^2 = \frac{1}{2}\frac{\omega_2}{\omega_1} \sum_{kq} \sum_{\boldsymbol{\epsilon}_1,\boldsymbol{\epsilon}_2} |U_{kq}(n_f j_f; n_i j_i)|^2, \quad (9)$$

if we assume that the incident light is unpolarized and that the polarization of scattered photons and the magnetic sublevel population of the residual ion remain unobserved. For such a setup of the experiment, the wave vector $\boldsymbol{k}_i$ of the incident photon is the only preferred direction of the overall system. Therefore, the emission of the scattered light can be

characterized by the (single) polar angle θ as defined with regard to this direction.

One can also calculate the total Raman scattering cross section if Eq. (9) is integrated over all directions of the outgoing photon:

$$\sigma(\omega_1) = \frac{1}{2}\frac{\omega_2}{\omega_1}\int \sum_{kq}\sum_{\epsilon_1,\epsilon_2} |U_{kq}(n_f j_f; n_i j_i)|^2 d\Omega. \quad (10)$$

The dependence of this cross section on the incoming photon energy arises from the reduced matrix elements (7) and (8). In Sec. IV A we study this energy dependence for selected hydrogenlike ions.

C. Alignment of a final ionic state

Until now, we have considered the total cross section and angular distribution of the photons of the Raman scattering process. We can also use the transition amplitude $M_{if}(\mu_i,\mu_f)$ to investigate the (magnetic sublevel) population $|n_f j_f \mu_f\rangle$ of the residual excited ion as often described in terms of so-called alignment parameters A_{kq}. In atomic collision studies, information about these parameters is typically obtained by analyzing the angular distribution and/or polarization of the subsequent decay photons. For example, the (angular and polarization) properties of the radiation emitted in the decay of states with $j_f = 3/2$ is governed by just a single (nontrivial) alignment parameter

$$A_{20} = \frac{\sigma(\mu_f = \pm 3/2) - \sigma(\mu_f = \pm 1/2)}{\sigma(\mu_f = \pm 3/2) + \sigma(\mu_f = \pm 1/2)}. \quad (11)$$

In this expression, the $\sigma(\mu_f) \equiv \sigma(n_f j_f \mu_f)$ is the cross section for the formation of a particular excited sublevel. To calculate these partial cross sections, we assume the quantization axis and hence the alignment parameter A_{20} to be defined along the incoming photon beam and that the scattered photons remain unobserved. For the excited state $|n_f j_f = 3/2\rangle$ and for unpolarized incoming light then, the partial cross section reads

$$\sigma(n_f, j_f, \mu_f) = \frac{1}{2}\frac{1}{2j_i+1}\frac{\omega_2}{\omega_1} \times \sum_{\mu_i,\epsilon_1,\epsilon_2}\int |M_{fi}(\mu_i,\mu_f)|^2 d\Omega. \quad (12)$$

Inserting this expression into Eq. (11), we find after some angular momentum algebra

$$A_{20} = \sqrt{5(2j_f+1)}\sum_{k'k''q'} (-1)^{k'+j_i+j_f}\sqrt{2k'+1} \times \langle k'q'20|k''q'\rangle \begin{Bmatrix} j_f & j_i & k' \\ k'' & 2 & j_f \end{Bmatrix} \times \sum_{KQ} \frac{\int U_{k'q'} U^{\dagger}_{k''q'} d\Omega}{\int U_{KQ} U^{\dagger}_{KQ} d\Omega}, \quad (13)$$

where, for the sake of brevity, we just use the notation $U_{kq} \equiv U_{kq}(n_f j_f; n_i j_i)$ for the irreducible tensor (5).

III. COMPUTATIONS

As seen from Eqs. (9), (10), and (13), the computation of the Raman scattering cross sections as well as the alignment of the residual ion requires knowledge about the reduced matrix elements $S^{12}_{j_v}(\omega)$ and $S^{21}_{j_v}(\omega)$. To compute these matrix elements, a summation over the intermediate states $|n_v j_v\rangle$ needs to be performed, which includes not only the bound but also the (positive- and negative-energy) continuum solutions of the Dirac equation. In the present work we perform this infinite summation by means of the relativistic Green's function [24,25]. By expanding the Green's function in terms of Laguerre polynomials, as suggested by Hylton and Snyderman [26], we were able to evaluate the amplitudes (7) and (8) analytically for all pairs of allowed multipoles $(L_1 p_1, L_2 p_2)$. Numerical approximations of these amplitudes for all (electric and magnetic) fields up to octupole order $L = 3$ are used in our calculations in Sec. IV and were found sufficient to guarantee the convergence of the reported results.

IV. RESULTS AND DISCUSSION

A. Total cross section

Total cross sections of the inelastic scattering of light on atoms and ions have been studied mainly for light systems in the past [5,6]. In this low-Z regime, the theoretical description of the Raman process was based on Schrödinger's equation and the electric dipole approximation for the coupling of the electrons to the radiation field. To better understand how the cross section $\sigma(\omega_1)$ is affected by relativity and the contributions of the higher multipoles, we applied Eqs. (5)–(10) and calculated the $1s_{1/2} + \gamma_1 \to n_f j_f + \gamma_2$ Raman scattering of light on selected hydrogenlike ions with nuclear charge in the range $1 \leqslant Z \leqslant 92$. In Fig. 1, for example, we display the total cross sections for neutral hydrogen as well as for hydrogenlike xenon and uranium ions, if they are excited to the $2s_{1/2}$ (black solid line), $2p_{1/2}$ (red dash-dotted line), and $2p_{3/2}$ (green dashed line) states. In all these computations, the $\sigma_{1s\to 2s}$, $\sigma_{1s\to 2p_{1/2}}$, and $\sigma_{1s\to 2p_{3/2}}$ cross sections were determined for incident photon energies ω_1 between the $1s \to 2l_j$ (excitation) and the $1s$ ionization threshold. For these energies of the incoming photons, moreover, our fully relativistic calculations are compared with the nonrelativistic predictions by Sadeghpour and Dalgarno [5] and Zon *et al.* [6] for the $1s_{1/2} \to 2s_{1/2}$ transition.

As seen from the figure, the cross section for the Raman scattering of light, if displayed as a function of the incident photon energy, exhibits a pronounced resonance structure. Resonances in the cross sections generally arise whenever the photon energy allows the excitation of a (real) intermediate state $|n_v j_v\rangle$ with energy $E_v = E_{1s} + \omega_1$, though with different strength and widths. From a simplified point of view, the Raman scattering then proceeds as a sequential excitation-and-decay process: $1s_{1/2} + \gamma_1 \to n_v j_v \to n_f j_f + \gamma_2$. For the $1s_{1/2} \to 2s_{1/2}$ Raman scattering on neutral hydrogen, for instance, we predict three peaks for incident photons with energies $0.75|E_{1s}| < \omega_1 < 0.97|E_{1s}|$, i.e., well below the $|E_{1s}|$ ionization threshold. In the leading electric dipole $E1E1$ approximation, these peaks are simply attributed to the $3p, 4p$, and $5p$ intermediate states whose energies are given by Bohr's

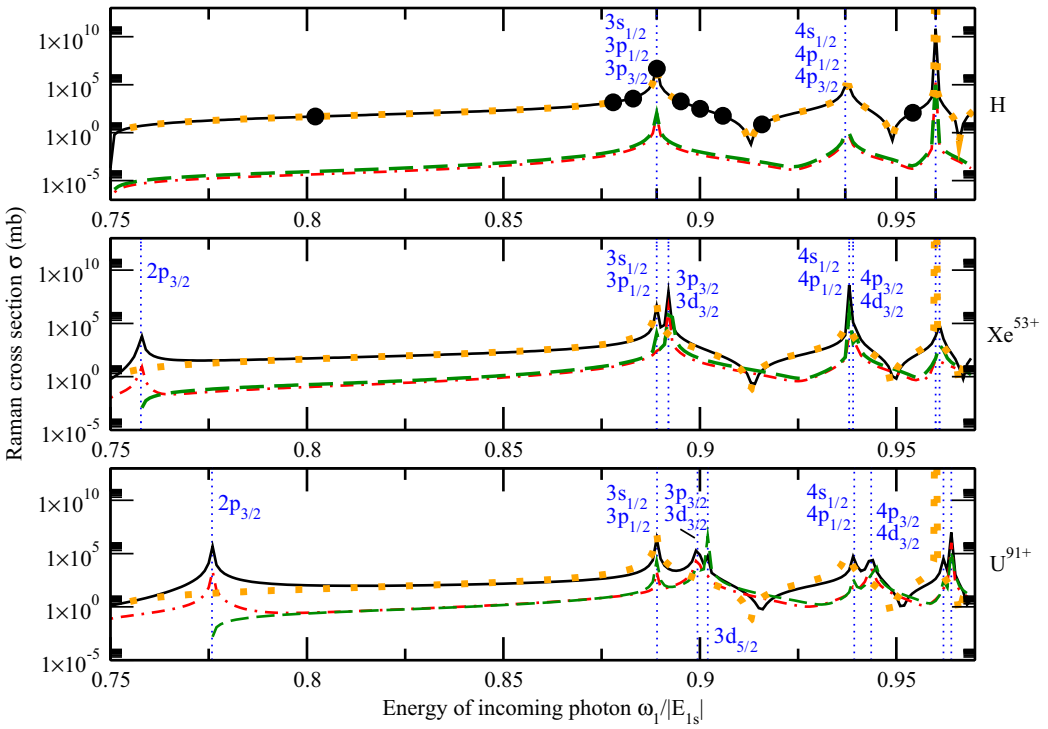

FIG. 1. (Color online) Total cross section (10) for the inelastic Raman scattering of photons on neutral hydrogen as well as hydrogenlike xenon and uranium ions. Results are shown as a function of the incident photon energy ω_1 in units of the $|E_{1s}|$ ionization threshold of the ions. Relativistic calculations were performed for the excitation of the targets from their ground state to the $2s_{1/2}$ (black solid line), $2p_{1/2}$ (red dash-dotted line), and $2p_{3/2}$ (green dashed line) levels. Moreover, the nonrelativistic predictions by Sadeghpour and Dalgarno [5] and Zon *et al.* [6], obtained for the $1s \to 2s$ scattering, are also displayed by closed circles and orange dotted lines, respectively. Positions of the intermediate-state resonances are marked by the vertical dotted lines.

formula $E_n = -1/2n^2$. However, this formula is no longer valid if the nuclear charge increases and hence relativistic effects become more and more important. For medium- and high-Z ions, the $n_v p_{1/2}$-$n_v p_{3/2}$ fine-structure splitting of the ionic levels becomes visible in the peak structure of the Raman cross section (see the middle and bottom panels of Fig. 1). A similar splitting in the resonances of the total cross sections is observed also for the $1s \to 2p_{1/2}$ and $1s \to 2p_{3/2}$ Raman scattering due to the interference of the direct scattering amplitudes with the excitation and decay via the $|n_v s\rangle$, $|n_v p\rangle$, and $|n_v d\rangle$ (real) intermediate states.

To better understand the influence of the relativistic and higher multipole corrections to the total cross section (10), one should consider not only the resonances but also the nonresonant region with $0.8 \lesssim \omega_1/|E_{1s}| \lesssim 0.87$, in which $\sigma(\omega_1)$ is a smooth function of the photon energy. In this region, the cross sections for an excitation to the $2s_{1/2}$, $2p_{1/2}$, and $2p_{3/2}$ ionic states behave rather different as the nuclear charges Z increases. For example, the Raman cross section $\sigma_{1s\to 2s}(\omega_1)$ for the simultaneous excitation of the electron to the $2s$ level changes only very little and is well reproduced by the nonrelativistic computations of Zon *et al.* [6], even for heavy ions. This behavior can be readily understood by the dominant $E1$ multipole components of the incident and outgoing photons in the scattering process $1s_{1/2} + \gamma_1 \to 2s_{1/2} + \gamma_2$, for which the $E1E1$ second-order transition amplitude $M_{if}^{E1E1}(\mu_i, \mu_f)$, i.e., if the summation in Eq. (5) is restricted to just one term with $p_1 = p_2 = 1$ and $L_1 = L_2 = 1$, depends weakly on Z [22,27,28]. This leads to a total cross section $\sigma_{1s\to 2s}(\omega_1)$ that varies very moderately along the hydrogen isoelectronic sequence. In contrast both the $\sigma_{1s\to 2p_{1/2}}(\omega_1)$ and $\sigma_{1s\to 2p_{3/2}}(\omega_1)$ cross sections for the excitation of the electron into the $2p_{1/2,3/2}$ shells increase by 3–4 orders of magnitude if the nuclear charge is raised from $Z = 1$ to $Z = 92$. This reflects again the behavior of the leading $M_{if}^{E1M1}(\mu_i, \mu_f)$ and $M_{if}^{E1E2}(\mu_i, \mu_f)$ scattering amplitudes that couple the $1s$ ground level to the excited $2p_{1/2,3/2}$ levels. These two amplitudes are approximately $\sim Z$, which results in the observed $\sim Z^2$ behavior of the cross section.

B. Angle-differential cross section

Besides the total cross sections (10), modern detectors also allow us to observe the angular distribution of inelastically scattered photons. In this section, therefore, we shall explore how the angular properties of the Raman scattered photons depend on both the nuclear charge Z and the energy ω_1 of the incident radiation. We here start with the energy $\omega_1 = 0.825|E_{1s}|$ of the incident photons for which the scattering process is not affected by the resonances. For this photon energy, Fig. 2 displays the angle-differential cross section for neutral hydrogen as well as hydrogenlike xenon and uranium ions. As before, computations have been performed for scattering with $1s_{1/2} \to 2s_{1/2}$ (left panels), $1s_{1/2} \to 2p_{1/2}$ (middle panels), and $1s_{1/2} \to 2p_{3/2}$ (right panels) simultaneous excitations of the ions. In this figure, moreover, we compare the results of the exact relativistic theory, including all

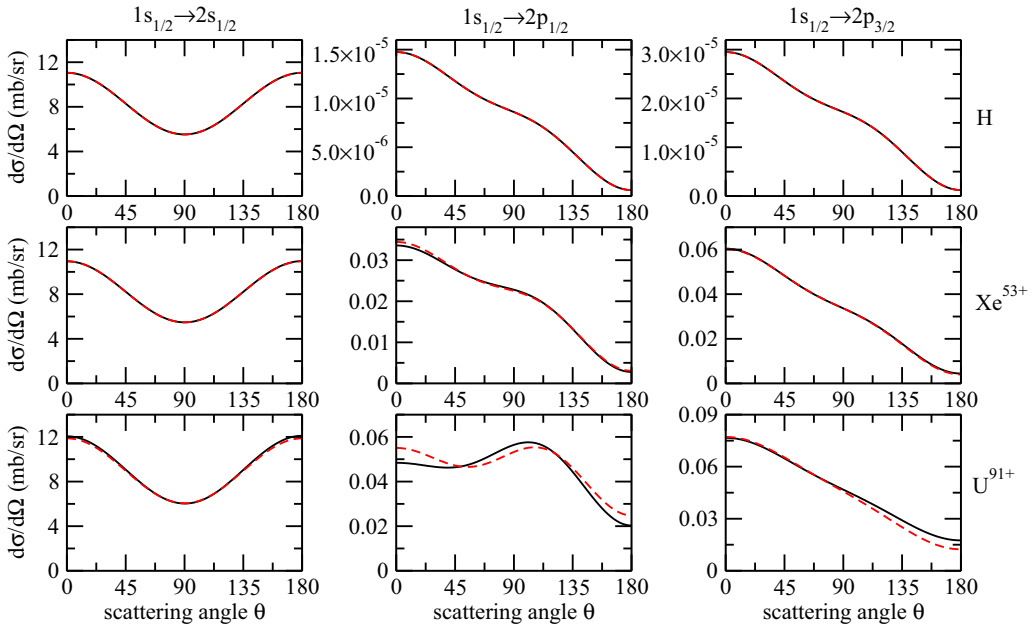

FIG. 2. (Color online) Angle-differential cross section (9) for the inelastic Raman scattering of unpolarized photons by neutral hydrogen (top panels), hydrogenlike xenon (middle panels), and hydrogenlike uranium (bottom panels) ions. Results are displayed for the $1s_{1/2} \to 2s_{1/2}$ (left column), $1s_{1/2} \to 2p_{1/2}$ (middle column), and $1s_{1/2} \to 2p_{3/2}$ (right column) transitions of the ions and for the photon energy $\omega_1 = 0.825|E_{1s}|$, well below the ionization threshold. Calculations within the leading $E1E1$ approximation for excitations into the $2s_{1/2}$ level and the $E1M1$-$E1E2$ approximation for the $2p_{1/2,3/2}$ levels (dashed line) are compared with those including all of the allowed multipoles (solid line).

the multipole components $(L_1 p_1, L_2 p_2)$ in the amplitude (5), with leading-order results, in which the summation over the multipole components is restricted to the single $E1E1$ term for $d\sigma/d\Omega_{1s\to 2s}$ and to the $E1M1$ and $E1E2$ terms for $d\sigma/d\Omega_{1s\to 2p_{1/2,3/2}}$, respectively.

As seen from the left panels of Fig. 2, the higher multipoles play almost no role in the inelastic Raman scattering that leads to the formation of the $2s_{1/2}$ excited state. In this particular case, both the rigorous relativistic theory (solid line) and the (leading) $E1E1$ approximation (dashed line) predict a proportional to $1 + \cos^2\theta$ angular distribution of the outgoing photons even for the heaviest ions. This shape also corresponds to the classical dipole radiation pattern and was predicted already by the nonrelativistic analysis by Zon *et al.* [6]. For the $1s_{1/2} \to 2p_{1/2}$ and $1s_{1/2} \to 2p_{3/2}$ Raman scattering, in contrast, the angular emission of the photons is much more sensitive to Z. For neutral hydrogen, for example, the $d\sigma/d\Omega_{1s\to 2p_{1/2}}$ and $d\sigma/d\Omega_{1s\to 2p_{3/2}}$ differential cross sections just differ by a factor of 2 from each other, owing to the statistical weights of the $2p_{1/2}$ and $2p_{3/2}$ levels, and both display a dominant emission of the scattered photons in the forward direction (see the middle and right columns of Fig. 2). Such an angular distribution is determined already by the leading $E1M1$ and $E1E2$ two-photon amplitudes, while the effects of higher multipoles remain negligible. As the nuclear charge Z increases, however, the higher-multipole contributions to the electron-photon interaction (3) become more important and give rise to an enhance scattering at angles $\theta \approx 100^\circ$ of the outgoing photons in the $1s_{1/2} + \gamma_1 \to 2p_{1/2} + \gamma_2$ Raman process. For the excitation to the $2p_{3/2}$ state of high-Z ions, in contrast, the Raman light is dominantly emitted under small angles $\theta \lesssim 60^\circ$, well in line with the leading-order ($E1M1$-$E1E2$) approximation.

Until now, we have discussed the Z behavior of the Raman angle-differential cross section for the nonresonant energy $\omega_1 = 0.825|E_{1s}|$ of the incident photons. In order to analyze how the $1s \to nl_j \to n_f l_{j_f}$ resonances affect the angular emission of the scattered photons, Fig. 3 presents calculations for the $1s_{1/2} \to 2s_{1/2}$ (left panels) and $1s_{1/2} \to 2p_{1/2}$ (right panels) Raman scattering in hydrogenlike uranium U^{91+} and for the three energies $\omega_1 = 0.888|E_{1s}|$, $0.890|E_{1s}|$, and $0.895|E_{1s}|$, respectively. While the first of these energies lies below the $1s_{1/2} \to 3s_{1/2}$ and $3p_{1/2} \to n_f l_{j_f}$ resonance energies of $\simeq 0.8891|E_{1s}|$, the other two energies are slightly above the resonance. As seen from Fig. 3, the shape of both the $d\sigma/d\Omega_{1s\to 2s_{1/2}}$ and $d\sigma/d\Omega_{1s\to 2p_{1/2}}$ differential cross sections changes drastically in this (energy) region. For example, in the $1s_{1/2} \to 2s_{1/2}$ process, the photons are scattered dominantly in the forward and backward directions with regard to the incoming light (beam) below the resonance for $\omega_1 = 0.888|E_{1s}|$, but have the highest scattering cross section in the perpendicular direction ($\theta = 90^\circ$) for $\omega_1 = 0.890|E_{1s}|$. If the energy of the incident photon is even higher at $\omega_1 = 0.895$, the nonresonant behavior starts to reappear. In order to understand this behavior, we note that, within the vicinity of the $1s \to 3p_{1/2} \to 2s$ resonance and the leading $E1E1$ approximation, the sum over the multipole components in the transition amplitude (4) and (5) is dominated by the reduced matrix element $S^{21}_{j_v=1/2}(\omega_1; E1, E1)$. At this resonance, moreover, the amplitude can be approximated by the single term

$$S^{21}_{j_v=1/2}(\omega_1; E1, E1) \sim \frac{\langle 2s_{1/2}||\boldsymbol{\alpha}\hat{\boldsymbol{a}}(E1)||3p_{1/2}\rangle\langle 3p_{1/2}||\boldsymbol{\alpha}\hat{\boldsymbol{a}}(E1)||1s_{1/2}\rangle}{E_{1s_{1/2}} - E_{3p_{1/2}} + \omega_1}, \quad (14)$$

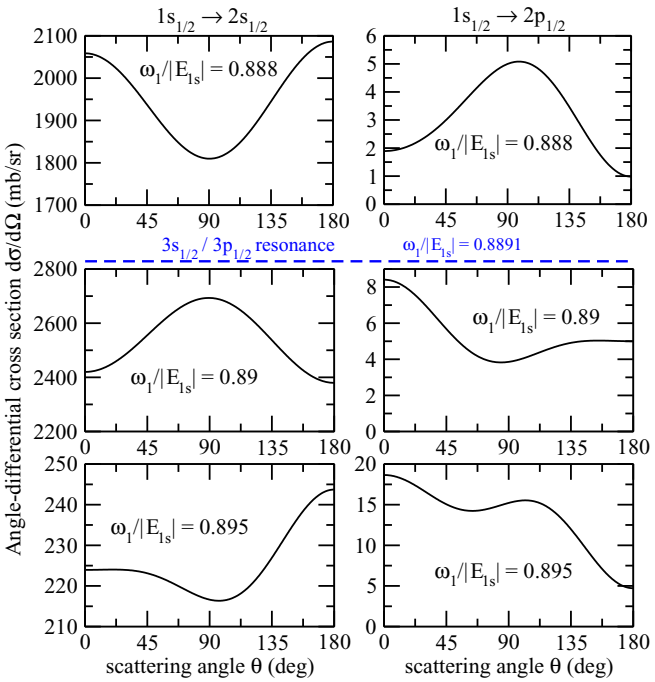

FIG. 3. (Color online) Angle-differential cross section (9) for the inelastic Raman scattering of unpolarized photons by hydrogenlike uranium U^{91+} ions. Results are shown for the $1s_{1/2} \to 2s_{1/2}$ (left column) and $1s_{1/2} \to 2p_{1/2}$ (right column) transitions of the ions and for the photon energies just below and above the $3s_{1/2}$, $3p_{1/2}$ resonances at $\omega_1/E_{1s} \simeq 0.8891$, the threshold for the $1s_{1/2} + \gamma_1 \to 3s_{1/2}/3p_{1/2} \to n_f j_f + \gamma_2$ scattering.

which changes its sign at the energy $\omega_1 = E_{1s_{1/2}} - E_{3p_{1/2}}$ of the incident photons. Since all the other reduced amplitudes S^{12} and S^{21} remain basically constant around this (resonance) energy, the sign change strongly affects the angular distribution of the photons in the $1s_{1/2} \to 2s_{1/2}$ Raman scattering process. For photons near the $1s_{1/2} \to 3p_{1/2}$ resonant excitation, this distribution can be written in the form

$$\left.\frac{d\sigma}{d\Omega}\right|_{\omega_1 \approx E_{3p_{1/2}} - E_{1s_{1/2}}} \sim C + S^{21}_{j_v=1/2}(\omega_1; E1, E1)\cos^2\theta, \quad (15)$$

where the parameter C is a smooth function of ω_1. This modified shape of the angle-differential cross sections near the $1s_{1/2} \to 3p_{1/2} \to 2s_{1/2}$ resonance only appears for mid- or high-Z ions. For low-Z ions, the peak in the angle-differential cross sections at the $3p_{3/2}$ resonance is very close to the peak at the $3p_{1/2}$ resonance and small changes in the incident photon energy change the sign of both the $S^{21}_{j_v=1/2}$ and the $S^{21}_{j_v=3/2}$ reduced matrix elements. The interplay of these different contributions stabilizes the angular shape in the resonant energy region.

The qualitative change in the angular emission of the inelastically scattered photons, caused by the $1s_{1/2} \to 3p_{1/2}$ resonance, can be observed experimentally in particular for heavy hydrogenlike ions. For the two scenarios displayed in Fig. 3, namely, the $1s_{1/2} \to 2s_{1/2}$ and $1s_{1/2} \to 2p_{1/2}$ Raman scattering on hydrogenlike ions, such experiments require x rays with photon energies ∼120 keV and with a spectral width of about 100 eV. X-ray radiation with these properties

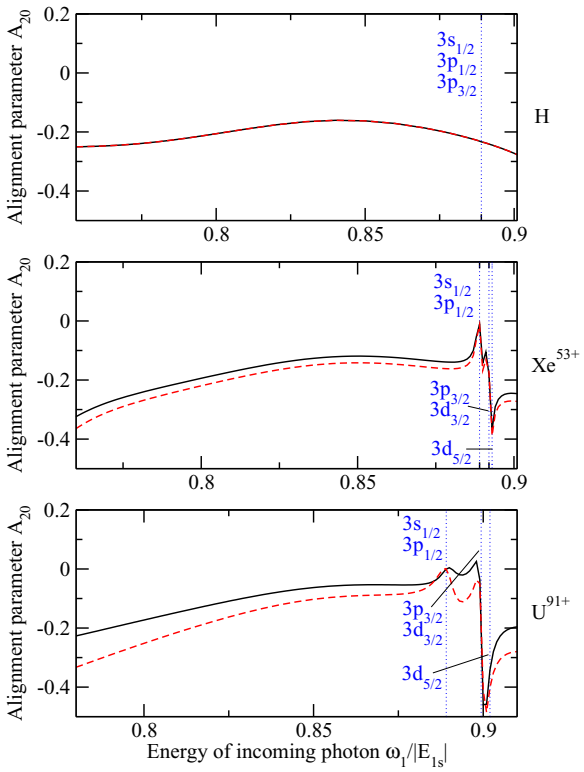

FIG. 4. (Color online) Alignment A_{20} of the $2p_{3/2}$ state of neutral hydrogen as well as hydrogenlike xenon and uranium ions following the inelastic Raman scattering of unpolarized photons. Calculations, performed within the leading-order approximation $E1M1$ and $E1E2$, are displayed by dashed lines and are compared with those including all of the allowed multipoles (solid lines).

is available today from modern synchrotron facilities, for instance, at PETRA III in Hamburg.

C. Alignment of the $2p_{3/2}$ state

As discussed before, the probability of exciting the ion into the $2p_{3/2}$ level by inelastic photon scattering increases rapidly as the nuclear charge is enlarged and this Raman scattering becomes pronounced especially for medium- and high-Z ions. Of course, the inelastic scattering of photons may also result in an alignment of the ion in the excited state, i.e., in an unequal population of the magnetic sublevels $|2p_{3/2}\mu_f\rangle$ with different moduli of the magnetic quantum number. Figure 4 displays the alignment parameter A_{20}, which characterizes the sublevel population of the ion in the $|2p_{3/2}\rangle$ state, for neutral hydrogen as well as Xe^{53+} and U^{91+} ions. Calculations, based on Eq. (13), have been performed for the incident photon energies below $0.9|E_{1s}|$, i.e., in an (energy) region in which the cascade feeding of the $2p_{3/2}$ level due to excitations of the ions into high-lying states can be neglected. For this region, a moderate negative alignment $-0.3 \lesssim A_{20} \lesssim 0$ is predicted for all three (ionic) targets. The alignment of the $|2p_{3/2}\rangle$ level is mainly determined by the leading $E1M1$ and $E1E2$ amplitudes, even though, especially for medium- and high-Z ions, the higher multipoles do reduce the (absolute value of) A_{20}.

V. SUMMARY AND OUTLOOK

In summary, a theoretical study has been performed for the inelastic (Raman) scattering of light on hydrogenlike ions. Special emphasis was placed on the total cross section, the angular distribution of the scattered photons, and the magnetic sublevel population of the residual ions. In order to evaluate these properties, we made use of Dirac's relativistic equation and second-order perturbation theory. Moreover, the summation over the complete (Dirac) spectrum, the intermediate ionic states, was performed by means of the Coulomb Green's function. Detailed computations are carried out for the $1s_{1/2} \to 2s_{1/2}$, $1s_{1/2} \to 2p_{1/2}$, and $1s_{1/2} \to 2p_{3/2}$ Raman scattering on neutral hydrogen as well as hydrogenlike xenon (Xe^{53+}) and uranium (U^{91+}) ions. The results of these calculations indicate that the $1s_{1/2} \to 2p_{1/2}$ and $1s_{1/2} \to 2p_{3/2}$ Raman scattering is negligible for low-Z systems but increases significantly for larger nuclear charge Z, an effect that can be attributed to the enhanced role of nondipole contributions to the electron-photon interaction.

Apart from the Z dependence, the total cross section for Raman scattering of light and for a particular excitation of the ion appears also to be quite sensitive to the energy of the incident light, showing pronounced enhancements at the resonant transitions of the ion to higher-lying states. These resonances can be interpreted of course as two-step process, in which the scattering proceeds via a well-defined intermediate state of the ions, together with the subsequent decay of the state of consideration. The positions of the resonances therefore reflect the fine structure and especially the level splitting of high-Z hydrogenlike ions. When compared with the total cross sections, similar or even larger effects of the resonance are found for the angle-differential cross sections. For the Raman scattering into the $2s_{1/2}$ state, for example, a remarkable shift in the angular distribution of the scattered photons was found, ranging from a dipolelike $1 + \cos^2\theta$ shape for nonresonant photon energies to an emission almost perpendicular to the direction of the incoming beam, if the (incoming) photon energy crosses the $1s_{1/2} \to 3p_{1/2}$ excitation energy.

Furthermore, we have investigated also the alignment of the residual ions, i.e., their magnetic sublevel population. A moderate alignment was found for a wide range of photon energies and can be attributed mainly to the $E1M1$ and $E1E2$ amplitudes. Information about the alignment of the ions can be derived, for instance, from angular- and polarization-resolved measurements of their subsequent Lyman-α_1 ($2p_{3/2} \to 1s_{1/2}$) decay. A theoretical analysis of this characteristic photon emission following the inelastic Raman scattering is left for future research.

ACKNOWLEDGMENTS

Stimulating discussions with R. Märtin are gratefully acknowledged. This work was supported by the Helmholtz Gemeinschaft (Nachwuchsgruppe VH-NG-421) and by the BMBF under Contract No. 05K13VHA.

[1] A. Smekal, Naturwissenschaften **11**, 873 (1923).
[2] C. V. Raman, Indian J. Phys. **2**, 387 (1928).
[3] P. P. Kane, Phys. Rep. **218**, 67 (1992).
[4] W. M. Saslow and D. L. Mills, Phys. Rev. **187**, 1025 (1969).
[5] H. Sadeghpour and A. Dalgarno, J. Phys. B **25**, 4801 (1992).
[6] B. A. Zon, N. L. Manakov, and L. I. Rapoport, Sov. Phys. JETP **28**, 480 (1969).
[7] Y. Gontier and M. Trahin, Phys. Rev. A **4**, 1896 (1971).
[8] Y. Heno, A. Maquet, and R. Schwarcz, J. Appl. Phys. **51**, 11 (1980).
[9] P. Bräunlich and P. Lambropoulus, Phys. Rev. Lett. **25**, 986 (1970).
[10] P. B. Hogan, J. L. Carlsen, F. M. J. Pichanick, S. J. Smith, and W. W. Smith, Phys. Rev. Lett. **37**, 990 (1976).
[11] H. M. Schmid, Astron. Astrophys. **211**, L31 (1989).
[12] H. Isliker, H. Nussbaumer, and M. Vogel, Astron. Astrophys. **219**, 271 (1989).
[13] J. P. J. Carney, R. H. Pratt, N. L. Manakov, and A. V. Meremianin, Phys. Rev. A **61**, 042704 (2000).
[14] R. H. Pratt, Radiat. Phys. Chem. **74**, 411 (2005).
[15] M. Jung, R. W. Dunford, D. S. Gemmell, E. P. Kanter, B. Krässig, T. W. LeBrun, S. H. Southworth, L. Young, J. P. J. Carney, L. LaJohn, R. H. Pratt, and P. M. Bergstrom, Phys. Rev. Lett. **81**, 1596 (1998).
[16] S. Fritzsche, P. Indelicato, and Th. Stöhlker, J. Phys. B **38**, S707 (2005).
[17] N. L. Manakov, A. A. Nekipelov, and A. G. Fainshtein, Sov. J. Nucl. Phys. **45**, 677 (1987).
[18] D. A. Varshalovich, A. N. Moskalev, and V. K. Khersonskii, *Quantum Theory of Angular Momentum* (World Scientific, Singapore, 1988).
[19] N. L. Manakov, A. V. Meremianin, and A. F. Starace, J. Phys. B **35**, 77 (2002).
[20] S. P. Goldman and G. W. F. Drake, Phys. Rev. A **24**, 183 (1981).
[21] A. Surzhykov, V. A. Yerokhin, T. Jahrsetz, P. Amaro, Th. Stöhlker, and S. Fritzsche, Phys. Rev. A **88**, 062515 (2013).
[22] A. Surzhykov, P. Indelicato, J. P. Santos, P. Amaro, and S. Fritzsche, Phys. Rev. A **84**, 022511 (2011).
[23] N. L. Manakov, A. V. Meremianin, and A. Maquet, J. Phys. B **33**, 4425 (2000).
[24] A. Surzhykov, P. Koval, and S. Fritzsche, Phys. Rev. A **71**, 022509 (2005).
[25] A. Maquet, V. Véniard, and T. A. Marian, J. Phys. B **31**, 3743 (1998).
[26] D. J. Hylton and N. J. Snyderman, Phys. Rev. A **55**, 2651 (1997).
[27] C. Szymanowski, V. Veniard, R. Taieb, and A. Maquet, Phys. Rev. A **56**, 700 (1997).
[28] C. Szymanowski, V. Veniard, R. Taieb, and A. Maquet, Europhys. Lett. **37**, 391 (1997).